Radiotracer Imaging of Peripheral Vascular Disease

Mitchel R. Stacy[1], Wunan Zhou[1], and Albert J. Sinusas[1,2]

[1]*Department of Internal Medicine, Yale University School of Medicine, New Haven, Connecticut; and* [2]*Department of Diagnostic Radiology, Yale University School of Medicine, New Haven, Connecticut*

CE credit: For CE credit, you can access the test for this article, as well as additional *JNMT* CE tests, online at https://www.snmmilearningcenter.org. Complete the test online no later than September 2018. Your online test will be scored immediately. You may make 3 attempts to pass the test and must answer 80% of the questions correctly to receive 1.0 CEH (Continuing Education Hour) credit. SNMMI members will have their CEH credit added to their VOICE transcript automatically; nonmembers will be able to print out a CE certificate upon successfully completing the test. The online test is free to SNMMI members; nonmembers must pay $15.00 by credit card when logging onto the website to take the test.

Peripheral vascular disease (PVD) is an atherosclerotic disease affecting the lower extremities, resulting in skeletal muscle ischemia, intermittent claudication, and, in more severe stages of disease, limb amputation and death. The evaluation of therapy in this patient population can be challenging, as the standard clinical indices are insensitive to assessment of regional alterations in skeletal muscle physiology. Radiotracer imaging of the lower extremities with techniques such as PET and SPECT can provide a noninvasive quantitative technique for the evaluation of the pathophysiology associated with PVD and may complement clinical indices and other imaging approaches. This review discusses the progress in radiotracer-based evaluation of PVD and highlights recent advancements in molecular imaging with potential for clinical application.

Key Words: peripheral vascular disease; SPECT; PET; perfusion; angiogenesis

J Nucl Med Technol 2015; 43:185–192
DOI: 10.2967/jnumed.112.115105

Peripheral vascular disease (PVD) is a progressive atherosclerotic process that results in stenosis or occlusion of noncoronary blood vessels. Although PVD can affect the arteries, veins, and lymphatics, primary interest has been focused on the effects on the arteries supplying the lower extremities. PVD affects approximately 8 million Americans (*1*) and an estimated 10% of the worldwide population (*2*), with increasing prevalence in older individuals (*3*). PVD has significant health implications, resulting in progressive limb ischemia that can lead to life-altering claudication, nonhealing ulcers, limb amputation, and, in severe cases, death (*2*). Despite these numbers and a close association with coronary artery disease, PVD still remains a relatively underdiagnosed disease (*4*).

Several techniques have been used for the evaluation and detection of PVD, including ankle–brachial indices, duplex ultrasound, MR imaging, CT angiography, SPECT, and PET (*5,6*). The ankle–brachial index is a widely applied diagnostic tool for the detection of PVD that uses the blood pressure differential between the upper and lower extremities to detect a functionally significant arterial obstruction, but this technique can be problematic in the setting of microvascular disease and medial calcification (*7,8*). Ultrasound is another relatively inexpensive, widely available, and fast diagnostic imaging tool compared with other imaging techniques, and these advantages have contributed to the routine application of this approach for screening and evaluation of PVD. Ultrasound, however, has limited penetration depth and is useful for assessment of only large-vessel blood flow (*6*). MR imaging has increased spatial resolution and tissue penetration and also allows for the evaluation of lower-extremity tissue perfusion and oxygenation in PVD patients (*9–11*). However, MR techniques are limited by their insensitivity to measure perfusion at rest and usually require exercise or protocols to provoke reactive hyperemia in order to generate an adequate augmentation of flow. Additionally, MR has decreased sensitivity for targeted molecular imaging and has fewer imaging probes available than nuclear imaging approaches (*12*). CT angiography allows for visualization of vessel morphology and is commonly used to assess the severity of PVD and to guide vascular interventions; however, quantitative tools for assessing the arterial tree in vivo are not readily available in the clinical setting (*13*).

Nuclear imaging approaches provide high sensitivity and, when applied with biologically targeted radiotracers, offer potentially novel methods for the investigation of PVD, with integration of perfusion and assessment of tissue

Received May 16, 2013; revision accepted Aug. 14, 2013.
For correspondence or reprints contact either of the following:
Mitchel R. Stacy, Yale University School of Medicine, Section of Cardiovascular Medicine, Dana-3, P.O. Box 208017, New Haven, CT 06520.
E-mail: mitchel.stacy@yale.edu
Albert J. Sinusas, Yale University School of Medicine, Section of Cardiovascular Medicine, Dana-3, P.O. Box 208017, New Haven, CT 06520.
E-mail: albert.sinusas@yale.edu

oxygenation, metabolism, or biologic processes such as angiogenesis (Table 1) (*6*). SPECT and PET are the primary nuclear imaging modalities, with SPECT being more established, less expensive, and more widely available. SPECT imaging also allows the simultaneous evaluation of multiple radiotracers. PET imaging provides increased sensitivity and resolution and generally involves radiotracers with shorter half-lives, resulting in lower levels of ionizing radiation exposure to patients. Both SPECT and PET, although providing higher sensitivity, also have lower spatial resolution when compared with CT and MR (submillimeter to ~1 mm resolution). The recent emergence of hybrid SPECT/CT and PET/CT systems, however, has allowed for the colocalization of high-sensitivity SPECT and PET imaging (within the picomolar range) with high-resolution anatomic imaging to optimally localize and quantify radiotracer uptake. Additionally, these hybrid imaging systems now permit correction of attenuation and partial-volume effects, allowing for more precise radiotracer quantification within anatomically defined regions of interest (*12*). This review discusses the progression of radiotracer-based assessment of PVD and highlights targeted imaging approaches that may offer new directions for investigation and clinical application.

RADIOTRACER IMAGING OF PVD

Assessment of Lower-Extremity Perfusion and Blood Flow

Impaired lower-extremity perfusion is a key pathophysiologic mechanism that drives the complications associated with PVD (*14*), making assessment of perfusion a valuable tool for evaluation of disease progression and the effectiveness of therapy. The first nuclear medicine studies examining lower-extremity skeletal muscle blood flow in patients with vascular disease evaluated the clearance rates of ^{24}Na-chloride (*15*), ^{133}Xe (*16*), and ^{99m}Tc-pertechnetate (*17*) after intramuscular injection of these radiotracers. The development of nuclear medicine in later years led to 2-dimensional imaging of microspheres and albumin that were radiolabeled with ^{99m}Tc (*18*), ^{131}I-sodium (*19*), and ^{111}In (*20*) to measure lower-extremity perfusion; however, these techniques were not ideal, as they required invasive intraarterial injections to evaluate blood flow during the first pass through the circulation. The need for techniques that did not require intraarterial injections ultimately led to the incorporation of ^{201}Tl as a perfusion agent in many imaging studies (*7,21*). ^{201}Tl is a diffusible tracer with biologic properties similar to potassium, allowing for transport into viable cells via the sodium–potassium pump (*22*), thus making the tracer uptake a reliable measure of both myocardial (*23*) and skeletal muscle perfusion (*21,24–26*). ^{201}Tl perfusion imaging can be performed after an intravenous injection at rest or during exercise and has a high first-pass extraction (~85%), providing a reliable estimate of flow over a wide physiologic range (*23*). Whole-body ^{201}Tl scintigraphy has been shown to be useful for evaluating perfusion abnormalities in the lower extremities of PVD patients at rest and during exercise stress (*25,26*), as well as in the identification of perfusion abnormalities in asymptomatic patients presenting with normal ankle–brachial indices (*7*). The assessment of PVD severity has traditionally been based on determining ratios of activity between nonstenotic and stenotic legs, or normalizing activity in lower-extremity regions of interest to whole-body activity in the presence of bilateral disease (*7,21,27*). With the emergence of 3-dimensional SPECT imaging systems, it was possible to more accurately detect and localize regions of lower-extremity ischemia under both rest and stress conditions with ^{201}Tl (*24*). One of the first lower-extremity imaging studies to use ^{201}Tl SPECT for the investigation of PVD evaluated stress profile curves from multiple transverse images in the leg during reactive hyperemia with normalization of regional activity to whole-body activity (Fig. 1) (*24*).

Although ^{201}Tl has proven to be an effective technique in multiple studies, the long half-life and less favorable imaging characteristics compared with ^{99m}Tc-labeled radiotracers has resulted in the adoption of these newer ^{99m}Tc-labeled perfusion tracers that provide better image quality (*28*). Additionally, ^{99m}Tc-labeled compounds demonstrate little redistribution, allowing for injections during treadmill exercise and measures of peak exercise perfusion at a delayed imaging time (*28*). The biodistribution and kinetics of the ^{99m}Tc-labeled compounds also make it possible to

TABLE 1
Radiotracers for Perfusion and Molecular Imaging of PVD

Modality	Perfusion/blood flow	Angiogenesis	Atherosclerosis
SPECT	^{201}Tl (*7,21,24–26*)	^{99m}Tc-NC100692 (*47,48*)	
	^{99m}Tc-sestamibi (*27,29,31*)	^{111}In-VEGF$_{121}$ (*45*)	
	^{99m}Tc-pyrophosphate (*76*)	^{125}I-c(RGD(I)yV) (*77*)	
	^{99m}Tc-tetrofosmin		
PET	^{15}O-water (*32,33,36,40*)	^{76}Br-nanoprobe (*50*)	^{18}F-FDG (*58–62*)
	C^{15}O$_2$ (*35*)	^{68}Ga-NOTA-RGD (*49*)	^{18}F-sodium fluoride (*66*)
	^{15}O$_2$ (*35,36*)	^{64}Cu-DOTA-CANF-comb (*52*)	^{11}C-acetate (*67*)
	^{13}N-ammonia (*34*)	^{64}Cu-DOTA-VEGF$_{121}$ (*46*)	^{64}Cu-DOTA-CANF (*65*)

CANF = C-type atrial natriuretic factor.

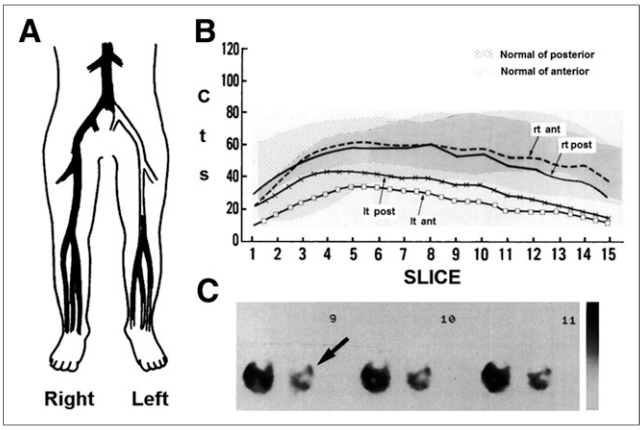

FIGURE 1. Arteriography (A) demonstrates unilateral PVD, which is confirmed by abnormal ^{201}Tl SPECT stress perfusion profile curves of anterior and posterior tibial muscle components of the left leg (B) as well as visual inspection of ^{201}Tl SPECT transverse images (C; perfusion defect noted by arrow). (Reprinted from (*24*).)

perform lower-extremity perfusion measurements in combination with myocardial perfusion (*27*). One ^{99m}Tc-labeled compound in particular, ^{99m}Tc-sestamibi, has been incorporated in several studies examining lower-extremity perfusion in PVD (*27,29,30*). Application of ^{99m}Tc-sestamibi imaging in patients has revealed improved sensitivity for detecting differences in resting perfusion between the lower extremities of PVD patients with unilateral disease and improved sensitivity compared with Doppler ultrasound for the detection of PVD (*31*). Preliminary data from our lab have shown that SPECT/CT imaging with ^{99m}Tc-tetrofosmin also has potential for assessing regional differences in lower-extremity perfusion in PVD patients with abnormal CT angiography findings and ankle–brachial indices (Fig. 2).

PET imaging can also assess lower-extremity blood flow in PVD (*32–36*). The primary PET radiotracer implemented in patient studies has been ^{15}O-water (*32,33,35,36*), which can freely diffuse into tissue (*37*) and has a short half-life (~2 min), making the tracer useful for repeated measurements of blood flow on the same individual in a single visit (33), at rest and during exercise (*38,39*), or during vasodilator stress (Fig. 3) (*32*). An ^{15}O-water rest–stress PET study found significant differences in flow reserve within the calves of PVD patients when compared with healthy volunteers, and these differences correlated with thermodilution-derived flow reserve values (*32*). Another study found significantly

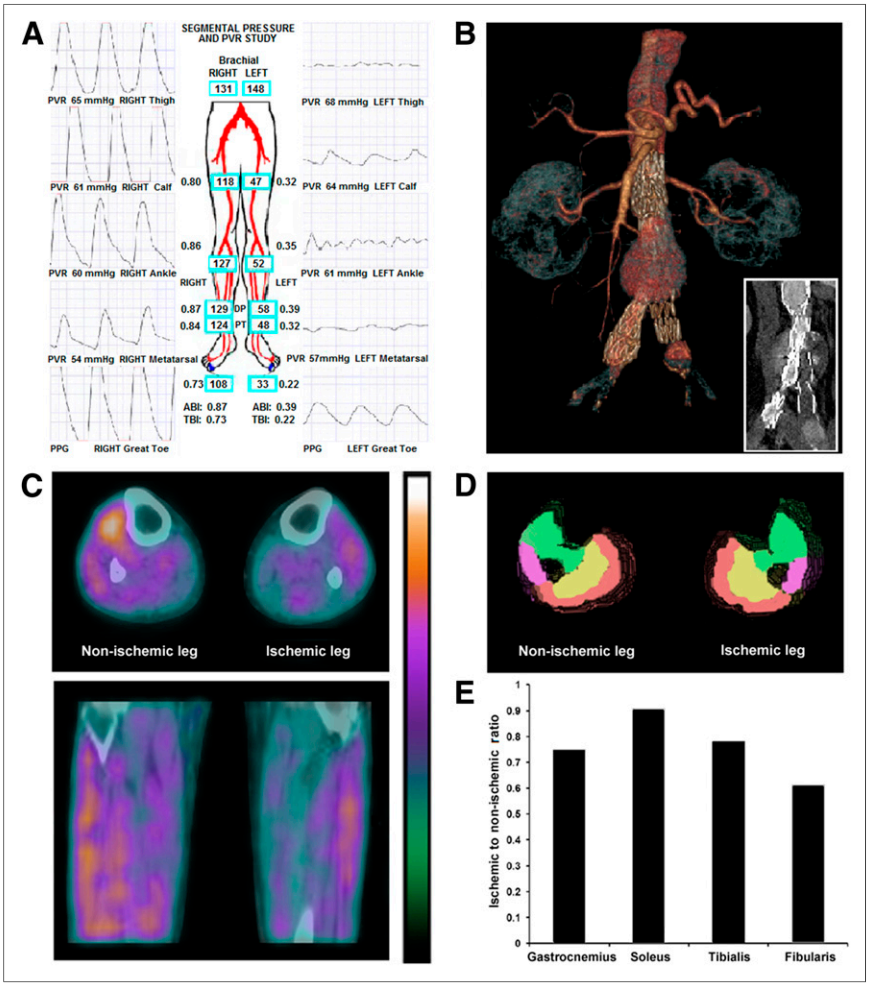

FIGURE 2. Multimodality evaluation with ankle–brachial indices (A), CT angiography (B), and hybrid ^{99m}Tc-tetrofosmin SPECT/CT (C) reveals impaired lower-extremity pressures and tissue perfusion in PVD patient with previously implanted aortoiliac stents (B). Segmentation of muscle groups into 3-dimensional regions of interest by CT attenuation images (D) confirmed differences in regional tissue perfusion between legs (E). Red = gastrocnemius; yellow = soleus; green = tibialis; purple = fibularis; ABI = ankle–brachial index; PPG = photoplethysmograph; PVR = pulse volume recording; TBI = toe–brachial index.

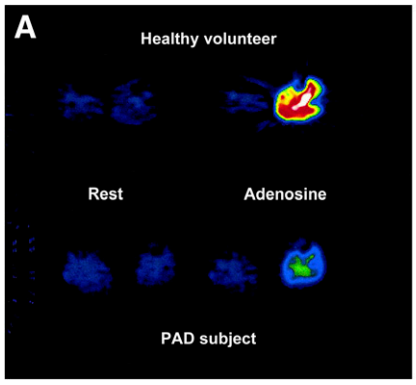

B

Lower Extremity Blood Flow

Subject no.	PET (GBq/mL) Base	Ad	FR
Healthy volunteers			
1	0.003	0.063	0.807
2	0.005	0.06	0.453
3	0.003	0.081	0.905
4	0.005	0.073	0.541
5	0.003	0.053	0.578
PAD subjects			
6	0.006	0.036	0.212
7	0.004	0.013	0.124
8	0.004	0.022	0.224
9	0.003	0.019	0.206
10	0.003	0.043	0.47

FIGURE 3. Lower-extremity PET $H_2{}^{15}O$ imaging of healthy subject and PVD patient during selective adenosine infusion into left leg (A). Baseline and adenosine stress blood flow was assessed, and flow reserve was expressed as ratio of adenosine flow to baseline flow (B). Flow reserve was significantly lower in PVD patients than in healthy subjects. (Reprinted from (*32*).).

reduced exercise-induced muscle blood flow in the distal legs of PVD patients who were referred for lower-limb amputation; these findings suggested that ^{15}O-water PET imaging may be a valuable tool for determining the level of subsequent amputations (*33*). Kalliokoski et al. (*39*) demonstrated that PET assessment of blood flow and oxygen uptake in lower-extremity skeletal muscle may be a useful tool for evaluating patient responses to exercise training programs. However, they observed considerable variability in baseline PET flow measurements, and therefore complementary techniques such as angiography may be required for thorough evaluation of patients with PVD.

PET imaging of preclinical animal models of PVD have been used to evaluate lower-extremity rest and stress blood flow and have demonstrated a high correlation ($r^2 = 0.98$) between PET- and microsphere-derived blood flow values (*34,40*). In a murine model of PVD, PET imaging with ^{13}N-ammonia has been used to assess acute and chronic changes in lower-extremity perfusion, showing a close correlation between PET perfusion results and histologic analysis of tissue fibrosis and necrosis (*34*).

Although PET imaging has proven to be useful for evaluating the lower extremities, the short half-life of available tracers can also present a limitation for lower-extremity PET imaging. Stress imaging with PET has traditionally required the use of exercise ergometers that are attached to scanners, as images must be acquired during or immediately after exercise stress. The recent development of an ^{18}F-labeled perfusion agent (flurpiridaz) for myocardial perfusion, however, may assist with the promotion of exercise PET imaging of both the heart and the lower extremities. The longer half-life (~110 min) of ^{18}F-flurpiridaz allows for tracer injection during peak treadmill exercise and then serial evaluation of myocardial and skeletal muscle stress perfusion. The high extraction fraction of ^{18}F-flurpiridaz in the myocardium may offer an advantage for evaluating lower-extremity skeletal muscle blood flow; however, this possibility still needs to be established (*41*).

Imaging of Angiogenesis

Targeted imaging of peripheral angiogenesis, in combination with lower-extremity perfusion imaging, may offer valuable information for in vivo assessment of the underlying pathophysiology associated with PVD. Angiogenesis, or the formation of new capillaries, is a complex process that involves various cell interactions and can be influenced by multiple stimuli, including lower-extremity ischemia (*42*). Radiotracer imaging of angiogenesis can focus on multiple regulatory targets, such as nonendothelial targets (e.g., monocytes, macrophages, and stem cells), endothelial cell targets (e.g., growth factor receptors, integrins, CD13, and cell adhesion molecules), extracellular matrix proteins, and proteases (*43*). Although many targets are potentially available for in vivo assessment of angiogenesis (Table 1), imaging studies investigating angiogenesis in the setting of limb ischemia have been primarily directed at vascular endothelial growth factor (VEGF) receptors and integrins, both of which play important roles in the process of angiogenesis (*44*).

VEGF ligands play a key role in the angiogenic process through binding to VEGF receptors (VEGF receptors 1–3), making VEGF receptors effective targets for the assessment of peripheral angiogenesis (*45,46*). A study by Lu et al. (*45*) demonstrated that targeted imaging of ^{111}In-labeled recombinant human $VEGF_{121}$, an angiogenic protein that is released in response to hypoxia and binds to VEGF receptors, could track ischemia-induced angiogenesis in a rabbit model. Another study used ^{64}Cu-labeled $VEGF_{121}$ to evaluate serial changes in VEGF receptor 2 expression in a murine model of hind limb ischemia with and without exercise training and found significantly higher levels of activity within ischemic limbs than in nonischemic contralateral limbs (*46*).

In addition to evaluating VEGF expression in preclinical models of PVD, studies have focused on targeted imaging of integrins (*47–50*). Integrins are transmembrane receptors that contribute to the angiogenic process through increased signal transduction as well as modulation of cell adhesion to the extracellular matrix (*44*). The $\alpha_v\beta_3$ integrin, which plays a key role in endothelial cell migration during angiogenesis (*51*), has gained significant attention for imaging of the angiogenic process (*47–50*). A study by Hua et al. (*47*) used a ^{99m}Tc-labeled peptide (NC100692) to target the $\alpha_v\beta_3$ integrin for serial assessment of angiogenesis

in a murine model of hind limb ischemia. Immunofluorescent staining confirmed specific targeting of the $\alpha_v\beta_3$ integrin on endothelial cells. Another study also revealed increased retention of ^{99m}Tc-NC100692 within segmented regions of interest in proximal and distal muscles of the ischemic hind limb, with peak relative retention occurring 1 wk after femoral artery occlusion (*48*). In addition to ^{99m}Tc-labeled compounds, cyclic Arg-Gly-Asp (cRGD)–labeled ^{68}Ga (*49*) and a ^{76}Br-labeled dendritic nanoprobe (*50*) have been used to assess $\alpha_v\beta_3$ expression in murine models of hind limb ischemia. Studies using ^{68}Ga- and ^{76}Br-labeled tracers have also observed significantly higher levels of tracer retention ($\alpha_v\beta_3$ expression) in ischemic limbs at 1 wk after occlusion.

A more recent study has shown the feasibility of targeted PET imaging of angiogenesis with a ^{64}Cu-labeled C-type atrial natriuretic factor–conjugated comblike nanoparticle that detects upregulation of natriuretic peptide clearance receptor (Fig. 4) (*52*). Natriuretic peptides are vascular homeostasis hormones that are secreted from heart and vasculature and function through interaction with their receptors, particularly natriuretic peptide clearance receptor (*53*). Liu et al. (*52*) compared PET nanoprobes developed for targeted and nontargeted PET imaging of natriuretic peptide clearance receptor in a murine model of hind limb ischemia. Targeted imaging with a receptor-specific nanoprobe proved to be highly sensitive to the angiogenic response when assessed 7 d after femoral artery ligation (Fig. 3), with immunohistochemistry confirming natriuretic peptide clearance receptor upregulation with colocalization in endothelial and smooth muscle cells.

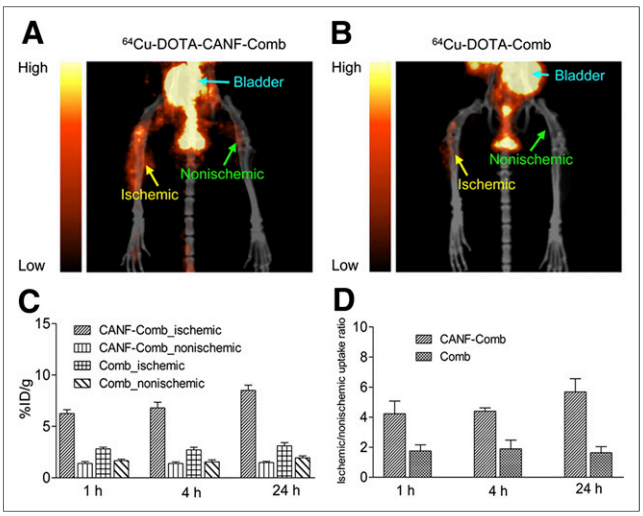

FIGURE 4. PET/CT imaging with ^{64}Cu-DOTA–C-type atrial natriuretic factor–comb (A) and ^{64}Cu-DOTA–comb (B) in mouse model of hind limb ischemia, 7 d after femoral artery occlusion. ^{64}Cu-DOTA–C-type atrial natriuretic factor–comb uptake was significantly higher than uptake of ^{64}Cu-DOTA–comb in ischemic limb when percentage injected tracer dose per gram of tissue (C) or ischemic-to-nonischemic leg ratios (D) were examined. (Reprinted from (*52*).) CANF = C-type atrial natriuretic factor.

Atherosclerosis Imaging

Although assessments of tissue perfusion, blood flow, and angiogenesis have potential for clinical application, recognition of unstable plaque that is vulnerable to rupture is another area of investigation. In recent years, the development of nuclear imaging probes for noninvasive assessment of plaque evolution and stability has grown substantially (Table 1) (*54*). The progression of plaque formation is generally characterized by expansive and restrictive vascular remodeling, with multiple signaling events and cell interactions contributing to these processes. Studies now regularly use atherosclerotic plaque localization and characterization obtained from CT and MR to facilitate quantification of radiotracer activity within lesions by normalization of tracer uptake in the vessel of interest to the blood activity in a remote artery. PET imaging offers spatial resolution superior to that of SPECT and therefore has been the favored modality for many in vivo imaging studies investigating atherosclerosis (*54,55*).

Among the currently available radiotracers for in vivo assessment of atherosclerosis, PET imaging of ^{18}F-FDG has attracted attention (*56*). ^{18}F-FDG is a glucose analog that is metabolized and converted to FDG-6 phosphate and subsequently trapped in the cytosol of metabolically active cells. This characteristic of ^{18}F-FDG has resulted in the use for targeted PET imaging of activated macrophages, which are key mediators of the inflammatory response (*57*). Several clinical studies suggest that ^{18}F-FDG imaging is highly reproducible (Fig. 5) (*58*) and correlates well with macrophage activity (*59*). However, a recent study did not find a significant correlation between ^{18}F-FDG uptake in peripheral artery plaque and subsequent immunohistochemical staining of CD68, a measure of macrophage content (*60*). Although there are conflicting results as to the direct association between ^{18}F-FDG uptake and plaque vulnerability, initial studies revealed an increased prevalence of vascular ^{18}F-FDG uptake with increasing age and atherosclerotic risk factors (*61,62*). Cardiovascular risk factors have also been correlated with increased ^{18}F-FDG uptake in specific peripheral arteries, making PET a potentially useful predictor of future cardiovascular events and tool for evaluating the effectiveness of medical therapy (*63*).

In addition to ^{18}F-FDG, other PET radiotracers have also been developed for the evaluation of atherosclerosis in animal models and patients. Tracers have focused on various targets associated with atherosclerosis, including inflammatory cells, markers of extracellular matrix remodeling, and mediators of angiogenesis (Table 1); however, ^{18}F-FDG is currently the only radiotracer that has been widely applied in the clinical setting (*54,57,64*). Few nuclear imaging studies have evaluated peripheral atherosclerosis to date (*58,60,61,65–67*), although ^{18}F-FDG patient imaging has been shown to be highly reproducible when performed 2 wk

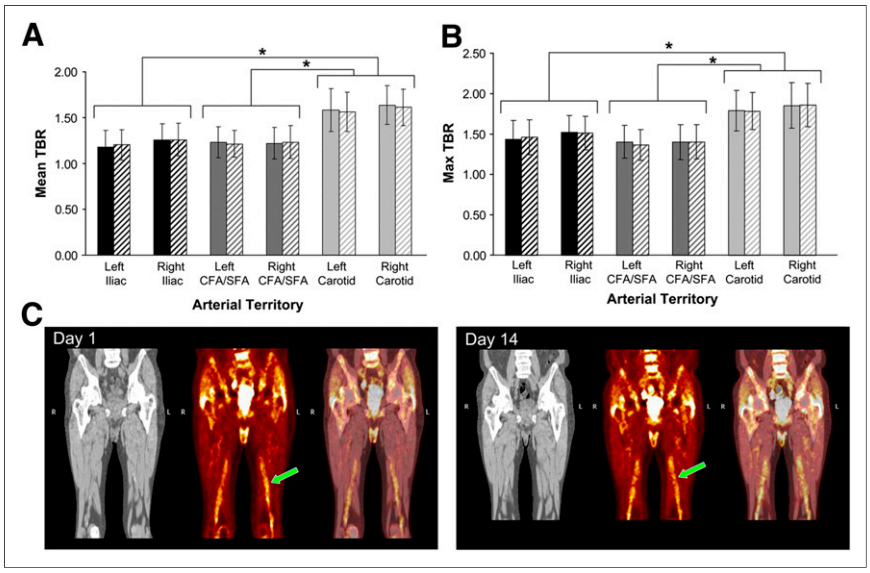

FIGURE 5. Analysis of mean (A) and maximum (B) ^{18}F-FDG tumor-to-background ratios within multiple arterial regions on day 1 (solid bars) and 14 d later (hatched bars). No significant differences were observed within arterial regions across time. Carotid artery uptake was significantly higher than ^{18}F-FDG uptake within lower-extremity arteries on days 1 and 14. ^{18}F-FDG PET (C, middle) fused with CT imaging (C, right) revealed similar uptake in femoral arteries on days 1 and 14 (noted by arrows). CFA = common femoral artery; SFA = superficial femoral artery; TBR = tumor-to-background ratio. *$P < 0.001$. (Reprinted from (*58*).)

apart (Fig. 5) (*58*). ^{18}F-labeled sodium fluoride has also been used to investigate atherosclerotic plaque in peripheral vessels, with uptake being highest in the femoral artery (*66*). Additional preclinical studies with ^{64}Cu-labeled natriuretic peptide and clinical studies using ^{11}C-acetate have demonstrated increased radiotracer uptake within atherosclerotic lesions (*65,67*).

Developing Applications for Radiotracer-Based Investigation of PVD

Evaluation of deep vein thrombosis (DVT) in the lower extremities is a developing application for imaging of PVD that has garnered recent attention (*68–71*). Venous ultrasound is currently the most accepted tool for evaluating DVT; however, ultrasound is largely dependent on both operator skill and patient characteristics (*72*). Therefore, a more sensitive or specific technique might assist in the guidance of antithrombotic therapy. PET imaging has shown significantly higher uptake of ^{18}F-FDG within thrombosed veins than within nonthrombosed veins, and ^{18}F-FDG uptake has also been negatively correlated with time of DVT symptom onset, suggesting that ^{18}F-FDG imaging may assist in the evaluation of DVT chronicity (*68*). Scintigraphy with the ^{99m}Tc-labeled peptide P280 (apcitide) has also been successfully applied in patients as a tool for detecting DVT (*69*). Based on the high affinity of the ^{99m}Tc-apcitide peptide to activated platelets, it may be possible to differentiate new from old thrombi, a clinically important distinction. ^{99m}Tc-apcitide imaging has been shown to possess high sensitivity and specificity for the detection of thrombi when compared with compression ultrasound and phlebography (*70*). Along with ^{99m}Tc-apcitide, another ^{99m}Tc-labeled peptide, recombinant tissue plasminogen, has also shown high sensitivity and specificity in the detection of thrombi (*71*). Together, these approaches may provide potential for improved detection and evaluation of lower-extremity DVT.

Hypoxia and acidosis may represent alternative markers for evaluation of PVD (*73,74*). Myocardial imaging with hypoxia markers has already proven to be effective and could be potentially translated to peripheral tissue to evaluate the balance of flow and oxygen consumption in ischemic limbs (*74*). The pH (low) insertion peptide, pHLIP, has emerged as a peptide that may be used to investigate changes in acidosis. At acidic pH levels, equilibrium is shifted toward the insertion of pHLIP into the cell membrane and results in tissue accumulation. Sosunov et al. (*75*) demonstrated that pHLIP can also be used to successfully target ischemic myocardium without requiring severe myocardial damage. Although there are currently no studies that have used pHLIP or hypoxia imaging in the investigation of PVD, future applications may enhance the understanding of the underlying pathophysiology of PVD and therapeutic interventions directed at improving angiogenesis, arteriogenesis, and tissue perfusion.

CONCLUSION

Approaches for radiotracer imaging of PVD continue to advance and show potential, with multiple molecular targets already available in preclinical models. Although many nuclear tracers have been developed, clinical application of molecular imaging in PVD has yet to reveal the full potential in patient populations. Continuing development of radiotracer imaging of PVD may provide effective, noninvasive techniques for evaluating serial responses to various forms of medical therapy, such as revascularization, exercise programs, and novel gene- or cell-based drug therapies. The high sensitivity of SPECT and PET imaging may be ideally suited for evaluation of these therapies and could complement anatomic and clinical indices for improved assessment of physiologic changes in PVD patients, providing potential guidance for vascular interventions as well as targeted delivery of drug therapies in the future.

ACKNOWLEDGMENT

We thank Da Yu Yu for assistance with the figures.

REFERENCES

1. Leeper NJ, Kullo IJ, Cooke JP. Genetics of peripheral artery disease. *Circulation.* 2012;125:3220–3228.
2. Peach G, Griffin M, Jones KG, Thompson MM, Hinchliffe RJ. Diagnosis and management of peripheral arterial disease. *BMJ.* 2012;345:e5208.
3. Gregg EW, Sorlie P, Paulose-Ram R, et al. Prevalence of lower-extremity disease in the US adult population >=40 years of age with and without diabetes: 1999-2000 national health and nutrition examination survey. *Diabetes Care.* 2004;27:1591–1597.
4. Hooi JD, Stoffers HE, Kester AD, et al. Risk factors and cardiovascular diseases associated with asymptomatic peripheral arterial occlusive disease. The Limburg PAOD study. Peripheral Arterial Occlusive Disease. *Scand J Prim Health Care.* 1998;16:177–182.
5. Pollak AW, Norton PT, Kramer CM. Multimodality imaging of lower extremity peripheral arterial disease: current role and future directions. *Circ Cardiovasc Imaging.* 2012;5:797–807.
6. Wolfram RM, Budinsky AC, Sinzinger H. Assessment of peripheral arterial vascular disease with radionuclide techniques. *Semin Nucl Med.* 2001;31:129–142.
7. Duet M, Virally M, Bailliart O, et al. Whole-body ^{201}Tl scintigraphy can detect exercise lower limb perfusion abnormalities in asymptomatic diabetic patients with normal Doppler pressure indices. *Nucl Med Commun.* 2001;22:949–954.
8. Goss DE, de Trafford J, Roberts VC, Flynn MD, Edmonds ME, Watkins PJ. Raised ankle/brachial pressure index in insulin-treated diabetic patients. *Diabet Med.* 1989;6:576–578.
9. Ledermann H-P, Schulte A-C, Heidecker H-G, et al. Blood oxygenation level-dependent magnetic resonance imaging of the skeletal muscle in patients with peripheral arterial occlusive disease. *Circulation.* 2006;113:2929–2935.
10. Pollak AW, Meyer CH, Epstein FH, et al. Arterial spin labeling MR imaging reproducibly measures peak-exercise calf muscle perfusion: a study in patients with peripheral arterial disease and healthy volunteers. *JACC Cardiovasc Imaging.* 2012;5:1224–1230.
11. Isbell DC, Epstein FH, Zhong X, et al. Calf muscle perfusion at peak exercise in peripheral arterial disease: measurement by first-pass contrast-enhanced magnetic resonance imaging. *J Magn Reson Imaging.* 2007;25:1013–1020.
12. Stacy MR, Maxfield MW, Sinusas AJ. Targeted molecular imaging of angiogenesis in PET and SPECT: a review. *Yale J Biol Med.* 2012;85:75–86.
13. Duran C, Bismuth J. Advanced imaging in limb salvage. *Methodist Debakey Cardiovasc J.* 2012;8:28–32.
14. Waters RE, Terjung RL, Peters KG, Annex BH. Preclinical models of human peripheral arterial occlusive disease: implications for investigation of therapeutic agents. *J Appl Physiol.* 2004;97:773–780.
15. Kety SS. Measurement of regional circulation by the local clearance of radioactive sodium. *Am Heart J.* 1949;38:321–328.
16. Lassen NA, Lindberg J, Munck O. Measurement of blood flow through skeletal muscle by intramuscular injection of xenon-133. *Lancet.* 1964;1:686–689.
17. Cutajar CL, Brown NJ, Marston A. Muscle blood-flow studies by the technetium ^{99m}Tc clearance technique in normal subjects and in patients with intermittent claudication. *Br J Surg.* 1971;58:532–537.
18. Rhodes BA, Greyson ND, Siegel ME, et al. The distribution of radioactive microspheres after intra-arterial injection in the legs of patients with peripheral vascular disease. *AJR.* 1973;118:820–826.
19. Coffman JD, Mannick JA. A simple objective test for arteriosclerosis obliterations. *N Engl J Med.* 1965;273:1297–1301.
20. Sheda H, O'Hara I. Study in peripheral circulation using I-131 and macroaggregated serum albumin. *J Exp Med.* 1970;101:311–314.
21. Siegel ME, Stewart CA. Thallium-201 peripheral perfusion scans: feasibility of single-dose, single-day, rest and stress study. *AJR.* 1981;136:1179–1183.
22. Gehring PJ, Hammond PB. The interrelationship between thallium and potassium in animals. *J Pharmacol Exp Ther.* 1967;155:187–201.
23. Pagnanelli RA, Basso DA. Myocardial perfusion imaging with ^{201}Tl. *J Nucl Med Technol.* 2010;38:1–3.
24. Oshima M, Akanabe H, Sakuma S, Yano T, Nishikimi N, Shionoya S. Quantification of leg muscle perfusion using thallium-201 single photon emission computed tomography. *J Nucl Med.* 1989;30:458–465.
25. Earnshaw JJ, Hardy JG, Hopkinson BR, Makin GS. Non-invasive investigation of lower limb revascularisation using resting thallium peripheral perfusion imaging. *Eur J Nucl Med.* 1986;12:443–446.
26. Hamanaka D, Odori T, Maeda H, Ishii Y, Hayakawa K, Torizuka K. A quantitative assessment of scintigraphy of the legs using ^{201}Tl. *Eur J Nucl Med.* 1984;9:12–16.
27. Kuśmierek J, Dąbrowski J, Bienkiewicz M, Szuminski R, Plachcinska A. Radionuclide assessment of lower limb perfusion using ^{99m}Tc-MIBI in early stages of atherosclerosis. *Nucl Med Rev.* 2006;9:18–23.
28. Kailasnath P, Sinusas AJ. Technetium-99m-labeled myocardial perfusion agents: are they better than thallium-201? *Cardiol Rev.* 2001;9:160–172.
29. Miles KA, Barber RW, Wraight EP, Cooper M, Appleton DS. Leg muscle scintigraphy with ^{99}Tc-MIBI in the assessment of peripheral vascular (arterial) disease. *Nucl Med Commun.* 1992;13:593–603.
30. Bajnok L, Kozlovszky B, Varga J, Antalffy J, Olvaszto S, Fulop T Jr. Technetium-99m sestamibi scintigraphy for the assessment of lower extremity ischaemia in peripheral arterial disease. *Eur J Nucl Med.* 1994;21:1326–1332.
31. Soyer H, Uslu I. A patient with peripheral arterial stenosis diagnosed with lower extremity perfusion scintigraphy. *Clin Nucl Med.* 2007;32:458–459.
32. Schmidt MA, Chakrabarti A, Shamim-Uzzaman Q, Kaciroti N, Koeppe RA, Rajagopalan S. Calf flow reserve with $H_2{}^{15}O$ PET as a quantifiable index of lower extremity flow. *J Nucl Med.* 2003;44:915–919.
33. Scremin OU, Figoni SF, Norman K, et al. Preamputation evaluation of lower-limb skeletal muscle perfusion with ^{15}O H_2O positron emission tomography. *Am J Phys Med Rehabil.* 2010;89:473–486.
34. Peñuelas I, Aranguren XL, Abizanda G, et al. ^{13}N-ammonia PET as a measurement of hindlimb perfusion in a mouse model of peripheral artery occlusive disease. *J Nucl Med.* 2007;48:1216–1223.
35. Depairon M, Zicot M. The quantitation of blood flow/metabolism coupling at rest and after exercise in peripheral arterial insufficiency, using PET and 15-O labeled tracers. *Angiology.* 1996;47:991–999.
36. Depairon M, Depresseux J-C, Petermans J, Zicot M. Assessment of flow and oxygen delivery to the lower extremity in arterial insufficiency: a PET-scan study comparison with other methods. *Angiology.* 1991;42:788–795.
37. Nuutila P, Kalliokoski K. Use of positron emission tomography in the assessment of skeletal muscle and tendon metabolism and perfusion. *Scand J Med Sci Sports.* 2000;10:346–350.
38. Ament W, Lubbers J, Rakhorst G, et al. Skeletal muscle perfusion measured by positron emission tomography during exercise. *Pflügers Arch.* 1998;436:653–658.
39. Kalliokoski KK, Knuuti J, Nuutila P. Relationship between muscle blood flow and oxygen uptake during exercise in endurance-trained and untrained men. *J Appl Physiol.* 2005;98:380–383.
40. Fischman AJ, Hsu H, Carter EA, et al. Regional measurement of canine skeletal muscle blood flow by positron emission tomography with $H_2{}^{15}O$. *J Appl Physiol.* 2002;92:1709–1716.
41. Maddahi J. Properties of an ideal PET perfusion tracer: new PET tracer cases and data. *J Nucl Cardiol.* 2012;19(suppl):S30–S37.
42. Simons M. Angiogenesis: where do we stand now? *Circulation.* 2005;111:1556–1566.
43. Orbay H, Hong H, Zhang Y, Cai W. PET/SPECT imaging of hindlimb ischemia: focusing on angiogenesis and blood flow. *Angiogenesis.* 2013;16:279–287.
44. Carmeliet P, Jain RK. Molecular mechanisms and clinical applications of angiogenesis. *Nature.* 2011;473:298–307.
45. Lu E, Wagner WR, Schellenberger U, et al. Targeted in vivo labeling of receptors for vascular endothelial growth factor: approach to identification of ischemic tissue. *Circulation.* 2003;108:97–103.
46. Willmann JK, Chen K, Wang H, et al. Monitoring of the biological response to murine hindlimb ischemia with ^{64}Cu-labeled vascular endothelial growth factor-121 positron emission tomography. *Circulation.* 2008;117:915–922.
47. Hua J, Dobrucki LW, Sadeghi MM, et al. Noninvasive imaging of angiogenesis with a ^{99m}Tc-labeled peptide targeted at alphavbeta3 integrin after murine hindlimb ischemia. *Circulation.* 2005;111:3255–3260.
48. Dobrucki LW, Dione DP, Kalinowski L, et al. Serial noninvasive targeted imaging of peripheral angiogenesis: validation and application of a semiautomated quantitative approach. *J Nucl Med.* 2009;50:1356–1363.
49. Jeong JM, Hong MK, Chang YS, et al. Preparation of a promising angiogenesis PET imaging agent: ^{68}Ga-labeled c(RGDyK)-isothiocyanatobenzyl1-1,4,7-triazacyclononane-1,4,7-triacetic acid and feasibility studies in mice. *J Nucl Med.* 2008;49:830–836.
50. Almutairi A, Rossin R, Shokeen M, et al. Biodegradable dendritic positron-emitting nanoprobes for the noninvasive imaging of angiogenesis. *Proc Natl Acad Sci USA.* 2009;106:685–690.
51. Brooks PC, Clark RAF, Cheresh DA. Requirement of vascular integrin alpha v beta 3 for angiogenesis. *Science.* 1994;264:569–571.
52. Liu Y, Pressly ED, Abendschein DR, et al. Targeting angiogenesis using a C-type atrial natriuretic factor-conjugated nanoprobe and PET. *J Nucl Med.* 2011;52:1956–1963.

53. Maack T, Suzuki M, Almeida FA, et al. Physiological role of silent receptors of atrial natriuretic factor. *Science.* 1987;238:675–678.
54. Sadeghi MM, Glover DK, Lanza GM, Fayad ZA, Johnson LL. Imaging atherosclerosis and vulnerable plaque. *J Nucl Med.* 2010;51(suppl):51S–65S.
55. Cavalcanti Filho JLG, de Souza Leão Lima R, de Souza Machado Neto L, Kayat Bittencourt L, Domingues RC, da Fonseca LMB. PET/CT and vascular disease: current concepts. *Eur J Radiol.* 2011;80:60–67.
56. Chen W, Bural GG, Torigian DA, Rader DJ, Alavi A. Emerging role of FDG-PET/CT in assessing atherosclerosis in large arteries. *Eur J Nucl Med Mol Imaging.* 2009;36:144–151.
57. Cocker MS, Mc Ardle B, Spence JD, et al. Imaging atherosclerosis with hybrid [^{18}F]fluorodeoxyglucose positron emission tomography/computed tomography imaging: what Leonardo da Vinci could not see. *J Nucl Cardiol.* 2012;19: 1211–1225.
58. Rudd JHF, Myers KS, Bansilal S, et al. Atherosclerosis inflammation imaging with ^{18}F-FDG PET: carotid, iliac, and femoral uptake reproducibility, quantification methods, and recommendations. *J Nucl Med.* 2008;49:871–878.
59. Rudd JHF, Warburton EA, Fryer TD, et al. Imaging atherosclerotic plaque inflammation with [^{18}F]-fluorodeoxyglucose positron emission tomography. *Circulation.* 2002;105:2708–2711.
60. Myers KS, Rudd JHF, Hailman EP, et al. Correlation between arterial FDG uptake and biomarkers in peripheral artery disease. *JACC Cardiovasc Imaging.* 2012;5:38–45.
61. Yun M, Yeh D, Araujo LI, Jang S, Newberg A, Alavi A. F-18 FDG uptake in the large arteries: a new observation. *Clin Nucl Med.* 2001;26:314–319.
62. Yun M, Jang S, Cucchiara A, Newberg AB, Alavi A. ^{18}F FDG uptake in the large arteries: a correlation study with the atherogenic risk factors. *Semin Nucl Med.* 2002;32:70–76.
63. Rominger A, Saam T, Wolpers S, et al. ^{18}F-FDG PET/CT identifies patients at risk for future vascular events in an otherwise asymptomatic cohort with neoplastic disease. *J Nucl Med.* 2009;50:1611–1620.
64. Hag AMF, Ripa RS, Pedersen SF, Bodholdt RP, Kjaer A. Small animal positron emission tomography imaging and in vivo studies of atherosclerosis. *Clin Physiol Funct Imaging.* 2013;33:173–185.
65. Liu Y, Abendschein D, Woodard GE, et al. Molecular imaging of atherosclerotic plaque with ^{64}Cu-labeled natriuretic peptide and PET. *J Nucl Med.* 2010;51:85–91.
66. Derlin T, Richter U, Bannas P, et al. Feasibility of ^{18}F-sodium fluoride PET/CT for imaging of atherosclerosis plaque. *J Nucl Med.* 2010;51:862–865.
67. Derlin T, Habermann CR, Lengyel Z, et al. Feasibility of ^{11}C-acetate PET/CT for imaging of fatty acid synthesis in the atherosclerotic vessel wall. *J Nucl Med.* 2011;52:1848–1854.
68. Rondina MT, Lam UT, Pendleton RC, et al. ^{18}F-FDG PET in the evaluation of acuity of deep vein thrombosis. *Clin Nucl Med.* 2012;37:1139–1145.
69. Muto P, Lastoria S, Varrella P, et al. Detecting deep venous thrombosis with technetium-99m-labeled synthetic peptide P280. *J Nucl Med.* 1995;36:1384–1391.
70. Dunzinger A, Hafner F, Schaffler G, Piswanger-Soelkner JC, Brodmann M, Lipp RW. ^{99m}Tc-apcitide scintigraphy in patients with clinically suspected deep venous thrombosis and pulmonary embolism. *Eur J Nucl Med Mol Imaging.* 2008;35:2082–2087.
71. Butler SP, Boyd SJ, Parkes SL, Quinn RJ. Technetium-99m-modified recombinant tissue plasminogen activator to detect deep venous thrombosis. *J Nucl Med.* 1996;37:744–748.
72. Zierler BK. Ultrasonography and diagnosis of venous thromboembolism. *Circulation.* 2004;109(12, suppl 1)I9–I14.
73. Naghavi M, John R, Naguib S, et al. pH heterogeneity of human and rabbit atherosclerotic plaques; a new insight into detection of vulnerable plaque. *Atherosclerosis.* 2002;164:27–35.
74. Sinusas AJ. The potential for myocardial imaging with hypoxia markers. *Semin Nucl Med.* 1999;29:330–338.
75. Sosunov EA, Anyukhovsky EP, Sosunov AA, et al. pH (low) insertion peptide (pHLIP) targets ischemic myocardium. *Proc Natl Acad Sci USA.* 2013;110: 82–86.
76. Yip TC, Houle S, Tittley JG, Walker PM. Quantification of skeletal muscle necrosis in the lower extremities using ^{99m}Tc pyrophosphate with single photon emission computed tomography. *Nucl Med Commun.* 1992;13:47–52.
77. Lee KH, Jung K, Song S, et al. Radiolabeled RGD uptake and alpha v integrin expression is enhanced in ischemic murine hindlimbs. *J Nucl Med.* 2005;46: 472–478.